Maffei 1 with the Hubble Space Telescope

R. Buta – University of Alabama

Marshall L. McCall – York University, Canada

Citation of published version:

Buta, R., McCall, M. (2003): Maffei 1 with the Hubble Space Telescope. *The Astronomical Journal*, 125(3). DOI: 10.1086/367789

The Astronomical Journal, 125:1150–1163, 2003 March

MAFFEI 1 WITH THE *HUBBLE SPACE TELESCOPE*[1]

R. Buta
Department of Physics and Astronomy, 206 Gallalee Hall, University of Alabama, Box 870324, Tuscaloosa, AL 35487;
buta@sarah.astr.ua.edu

and

Marshall L. McCall
Department of Physics and Astronomy, York University, 4700 Keele Street, Toronto, ON M3J 1P3, Canada;
mccall@yorku.ca

Received 2002 June 27; accepted 2002 December 15

ABSTRACT

High-resolution R, I, and Hα images of the center of Maffei 1, the nearest normal giant elliptical galaxy ($M_V^0 = -20.9$), have been acquired with the *Hubble Space Telescope*. At its distance of 3.0 Mpc, 1 pixel in the Planetary Camera field covers only 0.66 pc. The observations reveal that Maffei 1 is a "core type" elliptical galaxy, which is typical of intermediate to massive elliptical galaxies. A source of Hα emission has been discovered in the center. It is barely resolved, with a size of 1.2 pc and an ionized gas mass of only 29 $M_\odot$. Dust is very prominent west of the center in a complex irregular pattern. The correlation between the reddening and the deficiency in surface brightness reveals that the dust is most likely Galactic in origin and that the reddening law along the line of sight is typical of that for the diffuse interstellar medium. For the first time, globular clusters have been detected. Twenty field sources show slightly or significantly extended profiles relative to foreground stars. In I the absolute magnitude of the brightest is -9.6, which is comparable to that of M3 in the Milky Way. The spread in $R-I$ colors, as well the mean color, of these objects is greater than that found for Galactic globular clusters, which may be due in part to a metallicity difference compared with Galactic globular clusters and in part to the variable Galactic extinction across the Wide Field Planetary Camera 2 field. Fits of integrated analytic King models to three of the brighter candidates give core radii and concentration parameters that are comparable to those of Galactic globular clusters.

Key words: galaxies: elliptical and lenticular, cD — galaxies: photometry — galaxies: structure

1. INTRODUCTION

The heavily obscured galaxy Maffei 1 (Maffei 1968) is the nearest normal giant elliptical galaxy to the Milky Way (Fingerhut et al. 2003). Maffei 1 is a member of the IC 342 Maffei Group, a loose collection of more than a dozen heavily obscured galaxies toward $l = 140°$, $b = 0°$–$20°$ (Krismer, Tully, & Gioia 1995; Buta & McCall 1999, hereafter BM99). Maffei 1 is at a Galactic latitude of $-0.°5$, and early studies (Spinrad et al. 1971; Buta & McCall 1983) showed that it suffers from nearly 5 mag of visual extinction. The severe extinction causes Maffei 1 to appear extremely dim and small at blue and visual wavelengths, but if the extinction were removed it would be one of the biggest ($D_0 = 23'$) and brightest ($V_T^0 = 6.5$) galaxies in the sky (Fingerhut et al. 2003).

Considering the rarity of giant elliptical galaxies among nearby galaxy groups (see, e.g., de Vaucouleurs 1975), Maffei 1 is clearly an important object for detailed study, yet the high extinction and foreground star contamination have been a major setback for such studies. In particular, these have led to discordant estimates of the distance (e.g., Buta & McCall 1983; Luppino & Tonry 1993). This situation has now been remedied with the detailed study of Fingerhut et al. (2003), who used the correlation between the Mg_2 index and intrinsic $V-I$ color to get the most reliable extinction for Maffei 1 to date, $A_V = 4.67 \pm 0.19$ mag. In conjunction with surface photometry from BM99, this study also provided a new estimate of the distance to Maffei 1, 3.0 ± 0.3 Mpc, based on a weighted mean of its distance estimated from the fundamental plane and the D_n-σ relation.

Because of its Hubble type and its proximity, Maffei 1 is an obvious target for high-resolution observations with the *Hubble Space Telescope*. With the Wide Field Planetary Camera 2 (WFPC2), 1 pixel (0.″0455) in the PC1 corresponds to only 0.66 pc. This subparsec level of resolution is not normally achievable for giant elliptical galaxies, since the nearest examples tend to congregate in the Leo Group and the Virgo and Fornax Clusters, which are 3 to 5 times farther away. With this kind of resolution, Maffei 1 provides us with an opportunity to probe deeper into the core of a normal giant elliptical galaxy than has been possible with better known examples in these nearby clusters.

We report here on a detailed *Hubble Space Telescope* (*HST*) study of Maffei 1, based on R, I, and Hα images obtained with WFPC2. In particular, we obtain the surface brightness profile of Maffei 1 in to a radius of 0.″05, derive structural parameters of the core, examine dust structure near the center, and identify a possible nuclear gas disk. In addition, we report on the first detection of globular clusters in Maffei 1.

2. *HST* OBSERVATIONS OF MAFFEI 1

Maffei 1 was observed with *HST* on 2000 January 25 in two broadband filters, R (F675W) and I (F814W), and one narrowband filter, Hα (F656N). To avoid stray light

[1] Based on observations with the NASA/ESA *Hubble Space Telescope*, obtained at the Space Telescope Science Institute, which is operated by the Association of Universities for Research in Astronomy, Inc., under NASA contract NAS 5-26555.

patterns (see WFPC2 Handbook), careful attention was paid to the ORIENT angle to keep bright foreground stars out of positions that would lead to scattered light streaks or other effects. We chose an ORIENT angle in the range 80°–90°. The nucleus was centered in the PC1 field. To improve sampling of the point-spread function and thereby maximize our resolution of the center of the galaxy, we used the DITHER-TYPE=LINE option for all three filters. Thus, the galaxy was imaged at the input position and then reimaged after moving the telescope 5.5 PC pixels (or 2.5 WF pixels) along a 45° line. At each dither position, the integration time was used in a CR-SPLIT mode to facilitate the removal of cosmic rays. In *R* and *I*, individual exposures were kept short to minimize saturation of extremely bright stars and also to avoid any possible saturation in the core, especially in *I* (this turned out not to be a problem). The individual exposures were 230, 800, and 200 s for F675W, F656N, and F814W, respectively, while the total exposure times were 920, 3200, and 1600 s in the same filters.

The CR-SPLIT images at each dither position were cleaned of bad pixels by using the STSDAS routine WFIXUP. Since our main focus was on the very central area, the inherent uncertainties in using WFIXUP were inconsequential since few bad pixels affected the inner few arcseconds. The CR-SPLIT images were then combined using the IRAF routine CRREJ, which successfully removed most of the cosmic rays.

The DITHER package in IRAF was used for the combination of the dithered images. The task CROSSDRIZ was first used to produce a cross-correlation image of the two dither position images. From this, the task SHIFTFIND was used to derive the exact shifts between images. The shifts so derived showed that the dithering was successful, since the actual shifts are close to their nominal values. We also applied ROTFIND to determine whether a rotation angle was needed. However, the angle was determined to be less than 0°.05.

The task DRIZZLE was used to create a 1600 × 1600 subpixel image from the two input dithered images. We used a "drop size" (parameter pixfrac) of 0.6 pixel, slightly larger than the subpixel size (0.5 times the input pixel) in the output image. Each input data image was assigned a weight of 1.0. Each WFPC2 frame (PC1, WF2, WF3, and WF4) was then drizzled with its appropriate shifts, using geometrical distortion coefficients provided in the headers.

3. HIGH-RESOLUTION MORPHOLOGY

The STSDAS routine WMOSAIC was used to construct a mosaic image at each drizzle position. Then one was shifted to match the coordinates of the other to produce a full combined map for illustration. The inner section of the *I*-band mosaic is shown in Figure 1. In spite of the low Galactic latitude, there are remarkably few foreground stars

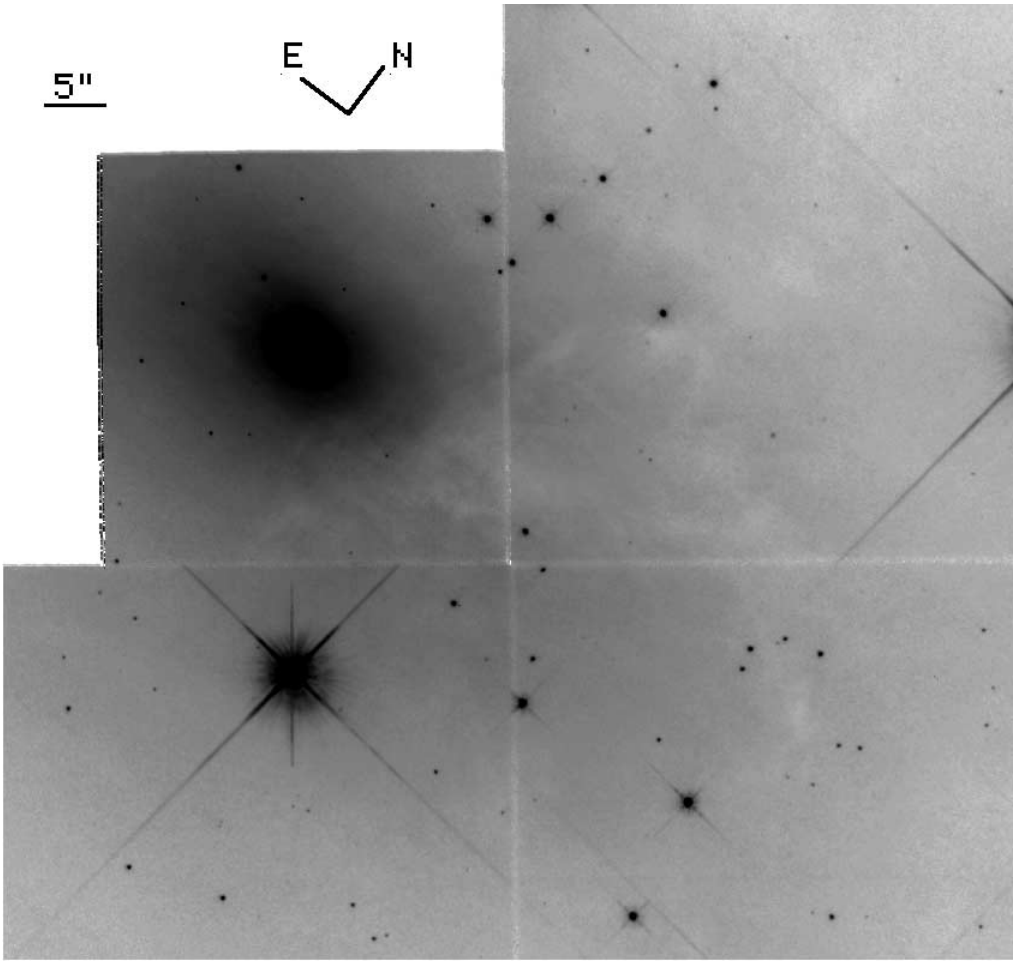

FIG. 1.—Negative F814W mosaic image of the central area of Maffei 1, showing the scale and orientation. The image is in logarithmic units. The position angle of the major axis is 84°.

in the image. However, in the west half of the PC1 field the image shows a complex pattern of obscuration, which can be traced into the three surrounding WF frames. To illustrate the structure better, we subtracted a two-dimensional model of the light distribution inferred from a combined ground-based and *HST* ellipse-fitted profile (see § 4.3). For the shape and orientation of this model we used an axis ratio of 0.729 and a position angle of 83°.9 from Table 4 of BM99. Figure 2 shows the difference image. Most of the obscuration is confined to the PC1 and WF4 frames. The large dust patch due west of center was discovered by Ford & Jenner (1971).

Figure 3 shows an $R-I$ color index map of the same area. There is reddening associated with the zones of flux deficiency (negative residuals) in Figure 2. The reddening is analyzed further in § 4.2, but note that the uniformity of color within 11″ suggests that the dust is fairly evenly distributed there. Thus, our perception of the light profile close to the nucleus should not be badly distorted by the dust.

Figure 4 (*left*) shows part of the drizzled *I*-band PC1 field, our highest-resolution image. In *I*, the core of Maffei 1 is soft, suggesting it is a core-type elliptical galaxy. This is confirmed in § 4.3. Figure 4 (*right*) shows the $R-I$ color index map of the same area. The main feature seen here is a blue nuclear point source. The F656N image sheds some light on the nature of this source. The F675W image was used to subtract the continuum from the F656N image. Three foreground stars were used to scale and register the F675W image for this purpose, as well as to match the point-spread functions. The resulting net Hα image is shown in Figure 5.

The main feature seen in the image is a small nuclear source. The FWHM of this source is 0″.11, compared with 0″.076 for foreground stars. Thus, the source is slightly resolved. After subtracting in quadrature the width of the stellar point-spread function (PSF) from that of the nucleus, the FWHM becomes 0″.080, which corresponds to 1.2 pc at a distance of 3.0 Mpc. In other words, we are resolving a source that is as small as the distance to Alpha Cen.

Using information from Holtzman et al. (1995), the net F656N flux from a circle of radius 11 dither pixels (0″.25), taking local background from 15 to 30 pixels, is 3.90×10^{-16} ergs cm^{-2} s^{-1}. Fingerhut et al. (2003) have measured the radial velocity of Maffei 1 to be $+66 \pm 5$ km s^{-1}. According to the WFPC2 Instrument Handbook, Version 3.0, the radial velocity of Maffei 1 places emission due to [N II] λ6583 in the low-sensitivity wing of the F656N filter, where the system throughput is only about 3% of that at the mean wavelength of 6564 Å. Phillips et al. (1986) have shown that the ratio F([N II] λ6583)/F(Hα) generally ranges from 1 to 3 for E and S0 galaxies and may be sensitive to absolute magnitude. To estimate the contribution of [N II] λ6583 to our measured flux, we use their Figure 16 and an

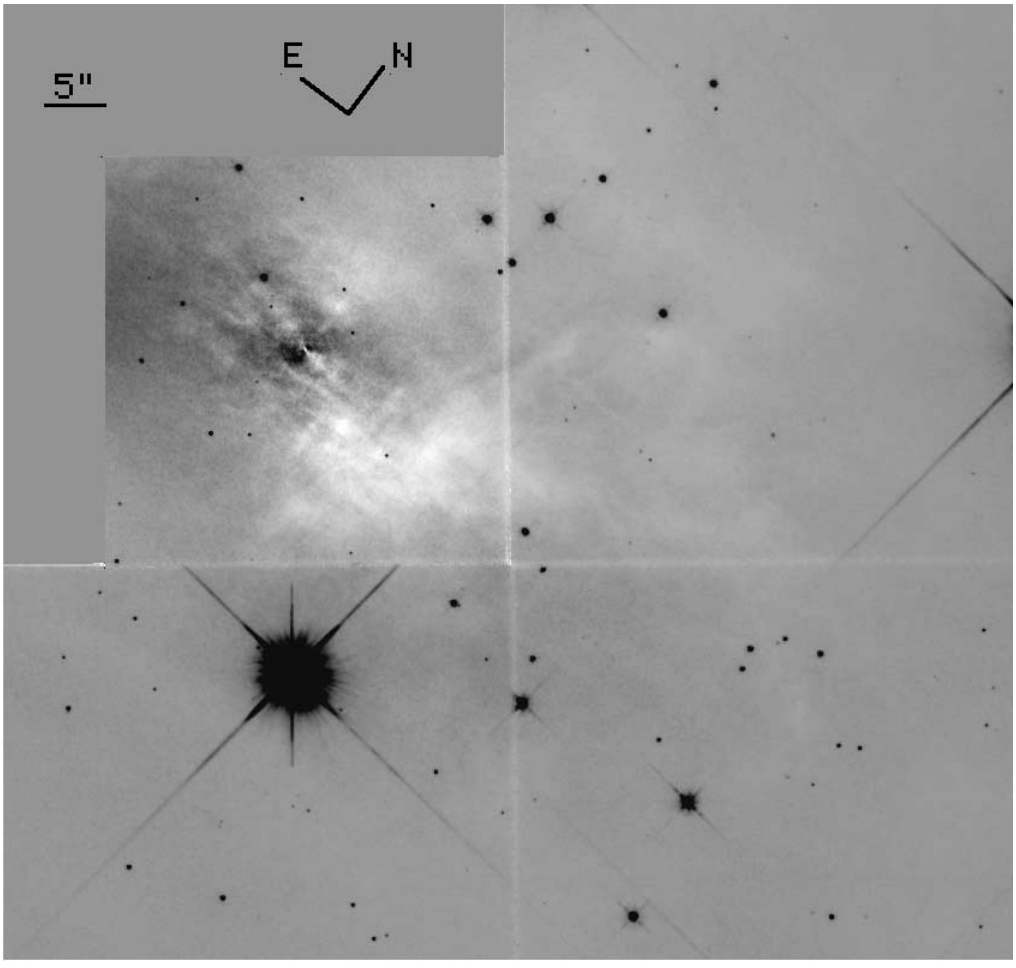

FIG. 2.—Negative F814W mosaic image of the same area as in Fig. 1, after subtraction of a model of the light distribution, revealing details of the dust structure in the inner regions and showing the scale and orientation. The image is in linear intensity units.

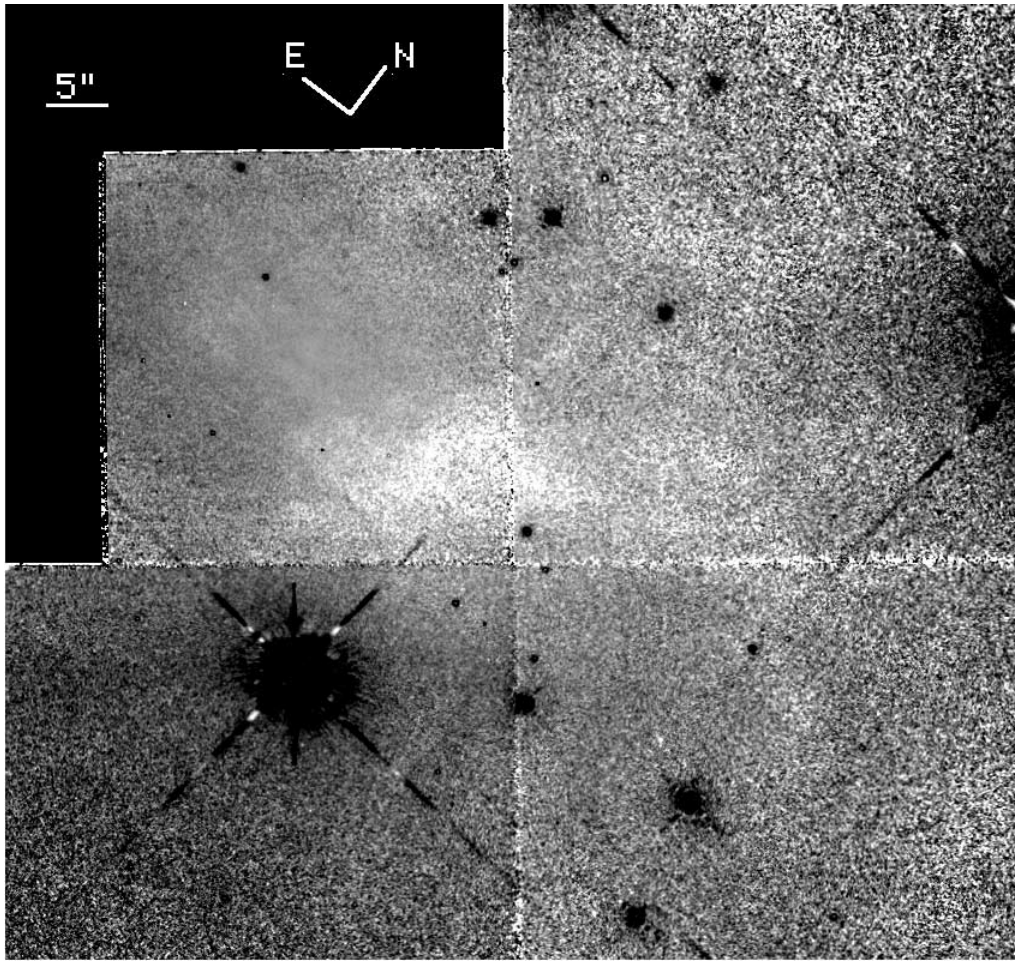

FIG. 3.—$R-I$ color index mosaic image of the same area as in Fig. 1, showing the scale and orientation. The image is in logarithmic units and coded such that redder regions are light and bluer regions are dark. The image shows evidence for variable reddening all across the field.

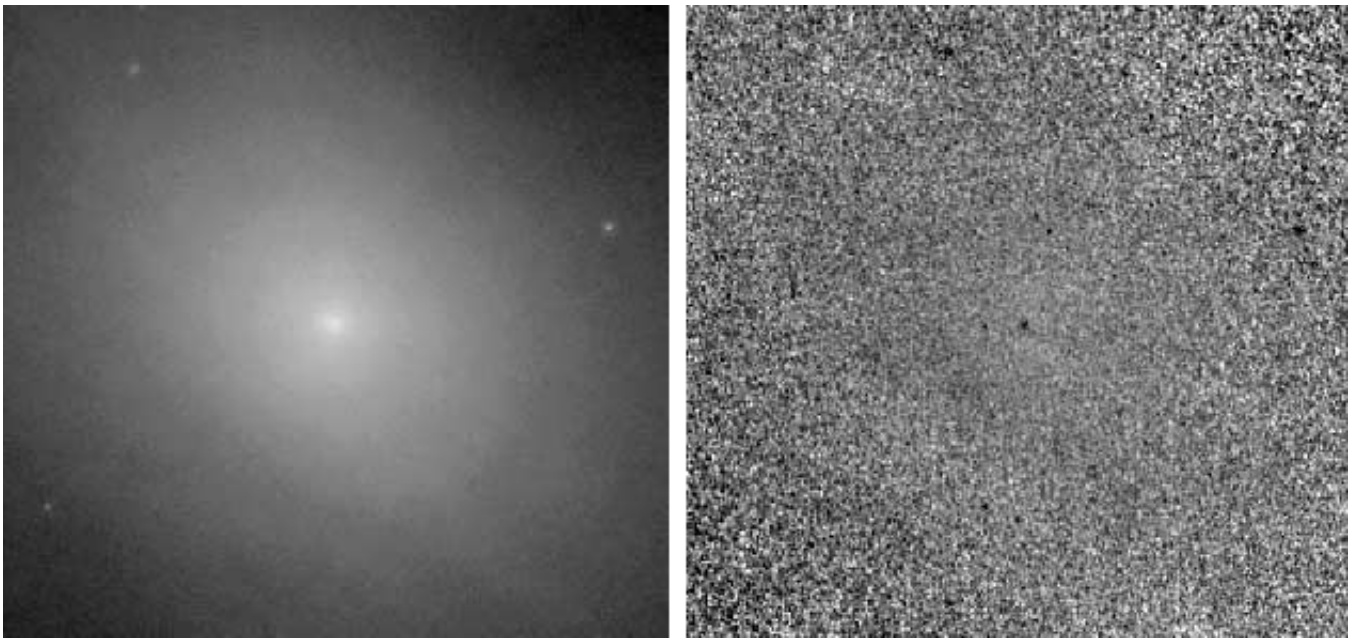

FIG. 4.—*Left*: I-band PC1 positive of the central $9\farcs6 \times 9\farcs0$ of Maffei 1. The image is in logarithmic units with the orientation being the same as in Figs. 1–3. *Right*: $R-I$ color index map of the same area as at left, revealing a small blue nuclear point source.

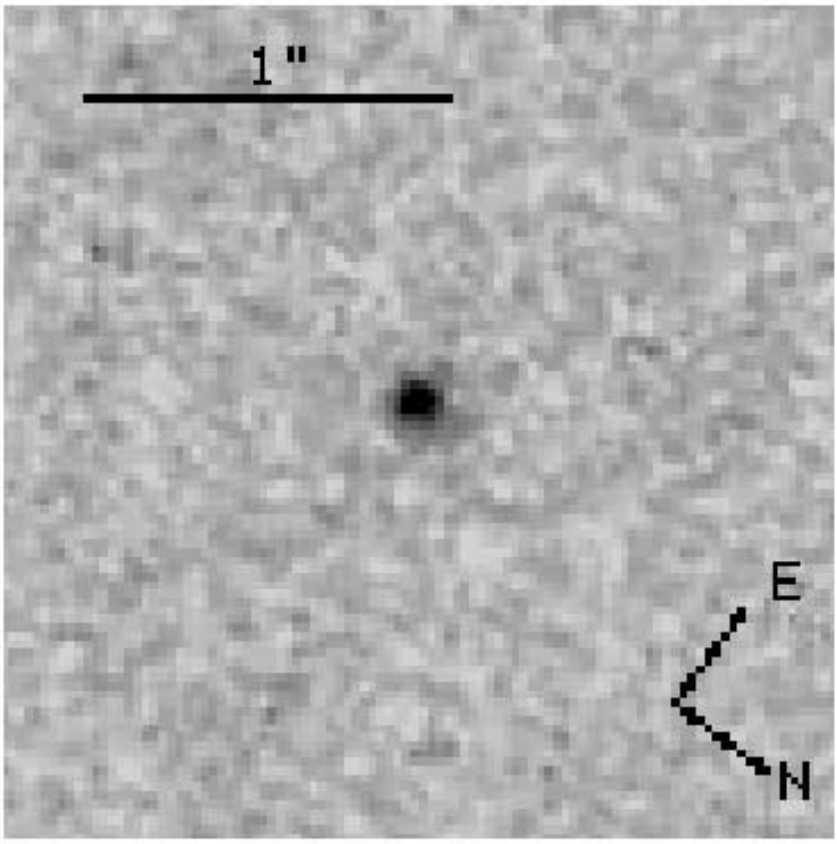

FIG. 5.—Net Hα negative of the inner $2''.275 \times 2''.275$ of Maffei 1, showing a weak nuclear point source with some extended emission to the north and east.

absolute B magnitude of -20.0; the expected ratio is 1.5 ± 0.5. For this ratio, [N II] λ6583 would contribute approximately 5% of our measured Hα flux. Thus, we estimate a net apparent Hα flux of 3.71×10^{-16} ergs cm^{-2} s^{-1}. Fingerhut et al. (2003) estimate that the optical depth at 1 μm is 1.69 ± 0.07. Based upon the monochromatic reddening law of Fitzpatrick (1999), parameterized to give $R = 3.07$ when integrated over the spectrum of Vega (see McCall 2002), $A_{\mathrm{H}\alpha} = 3.69$ mag. The total corrected Hα luminosity of the nuclear source is $L_c(\mathrm{H}\alpha) = 1.19 \times 10^{37}$ ergs s^{-1} for a distance of 3.0 Mpc.

The mass of the nuclear ionized gas can be estimated from the total Hα luminosity by using equation (3) of Phillips et al. (1986). For the same electron density ($N_e = 10^3$ cm^{-3}) and temperature ($T = 10^4$ K) used by those authors, we estimate a nuclear ionized gas mass of $\approx 29\ M_\odot$. This is a low value compared with that of the E and S0 galaxies observed by Phillips et al. In Maffei 1, we are able to easily detect a nuclear source of lower mass than was possible from ground-based observations of more distant galaxies.

4. PROFILE DERIVATION AND ANALYSIS

The high Galactic extinction toward Maffei 1 and the mismatch between the effective wavelengths of the WFPC2 filters and the standard *RI* ground-based filters means that we cannot transform the raw intensities for Maffei 1 directly to the standard system. As emphasized by Holtzman et al. (1995), it is essential to correct the natural WFPC2 magnitudes for extinction before transforming to the standard system. Integration of response curves over an appropriately extinguished integrated spectral energy distribution for an elliptical galaxy gives extinctions $A_{\mathrm{F675W}} = 3.51$ mag and $A_{\mathrm{F814W}} = 2.63$ mag (see McCall 2002). For the actual transformation to the standard Cousins R and I systems we use equation (8) and the $R-I$ calibration equations in Table 7 of Holtzman et al. (1995). A constant of 0.1 mag must be added to the zero points of that table to correct to infinite aperture (Holtzman et al. 1995). No corrections for charge transfer efficiency (Whitmore, Heyer, & Casertano 1999) are applied. These should be small in the PC1 field in any case, because of the high background (especially in I).

4.1. *Sky Background Level Determinations*

Maffei 1 fills the entire WFPC2 field, which makes direct determination of the background level difficult. Indirect estimates of 0.29 ADU per dithered pixel and 0.42 ADU per dithered pixel for R and I, respectively, can be deduced using information in Tables 6.1 and 6.3 of the WFPC2 Handbook. Although we expect the background to be low compared with the high surface brightness inner regions, these nominal values of the sky level in each filter are very likely underestimates since Maffei 1 is viewed against the Milky Way. Thus, we have used the ground-based folded major-axis surface brightness profile in Figure 29 of BM99 to independently estimate the background level in I and to infer that in R.

Figure 6 shows the resulting WFPC2 R and I profiles derived from the mosaic images. We used a major-axis position angle of 83°.9 (BM99) to define these profiles. On

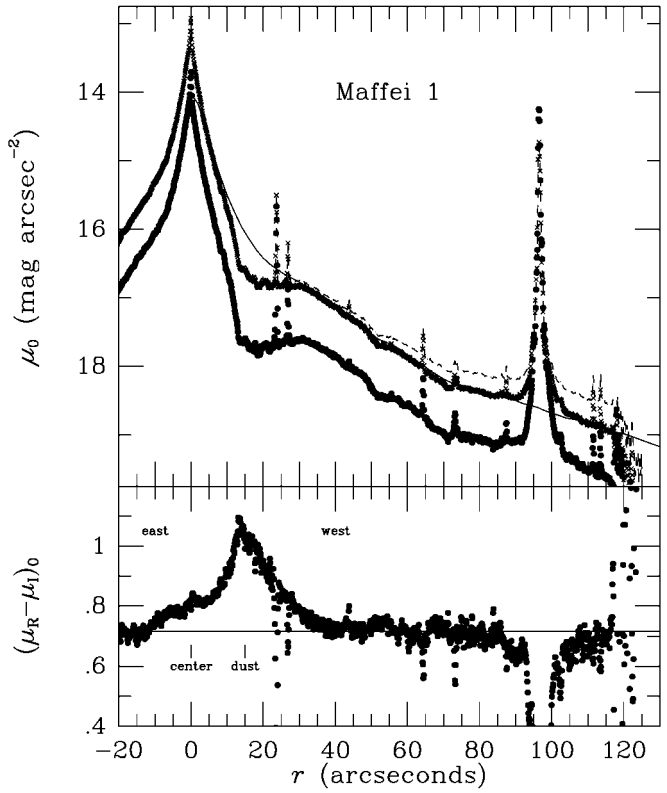

FIG. 6.—Major-axis surface brightness and color profiles of Maffei 1 from mosaic images. Crosses refer to the *I*-band WFPC2 profile while circles refer to the *R*-band WFPC2 profile. *Top*: Folded major-axis *I*-band profile from BM99 (*solid curve*), and the *I*-band WFPC2 profile (*dashed curve*) that would be obtained if we used a sky background inferred from the WFPC2 manual.

the west side this axis cuts through the dust patch at $r = 15''$, where a major dip in surface brightness and a hump in the color index are seen. Figure 6 compares the BM99 *I*-band profile (*solid curve*) with the WFPC2 profile (*dashed curve*) after subtracting 0.42 ADU pixel^{-1} from the latter. As expected, this choice of sky background gives a profile that is too bright in the outer radii compared with the BM99 profile. A much better match (away from the dust patch) is obtained for a background level of 0.84 ADU pixel^{-1} (Fig. 6, *crosses*). This background level is twice that which we inferred from the WFPC2 manual. Inside $r = 30''$, such a large uncertainty in the background nevertheless has little impact on the derived *I*-band surface brightnesses.

For the *R* band, we infer the background level by requiring that there be little color gradient outside the inner $10''$ and the obvious dust lanes, which is a reasonable assumption for an elliptical galaxy. This leads to a sky level of 0.526 ADU per dithered PC1 pixel, which is also nearly twice the nominal value inferred from the WFPC2 manual.

As noted by the referee, these estimates of the sky background are not as straightforward as our analysis might imply. The mismatch between the ground-based *I*-band filter used for the BM99 profile and that used for WFPC2 means that we cannot get a precise background estimate for the latter observations simply by comparing them with the former observations. Nevertheless, for our purposes, the procedure we have used is still better than assuming WFPC2 manual values and should be adequate since we are interested mainly in the surface brightnesses in the PC1 field, where the effect of the background uncertainty is low.

4.2. *Location of Dust Patches*

The location of the dust patches seen in the inner parts of Maffei 1 is important because it affects how we interpret the galaxy. If the dust is internal to Maffei 1, it would mean Maffei 1 belongs to the unusual class of dust lane elliptical galaxies (see Goudfrooij 1995) and may have suffered some kind of accretion event.

To elucidate the dust's location, we analyze a cut along the major axis out to a radius of $20''$ on either side of the nucleus. On the west side, this profile passes through the main dust lane, while on the east side no major dust features affect it. To improve the signal-to-noise ratio, the intensities are averaged along an elliptical contour within a cone whose half-angle is 5°. The contour is a segment of an ellipse having axis ratio 0.729 and major-axis position angle 83°.9. To work in the standard *RI* system, we correct the natural profiles for the adopted Galactic extinction from Fingerhut et al. (2003). Our remaining analysis is differential. We assume that the east side is the unextinguished side (after correction) and derive differential extinction and reddenings as follows:

$$A_R(r) = \mu_R^W(r) - \mu_R^E(r) \ ,$$

$$A_I(r) = \mu_I^W(r) - \mu_I^E(r) \ ,$$

$$E(R-I) = A_R - A_I \ .$$

Here μ_R^W and μ_I^W refer to the surface brightnesses at radius r on the west side of the major axis while μ_R^E and μ_I^E refer to those on the east side. Figure 7 shows the east and west profiles, their corresponding color profiles, and the ratio $A_R/E(R-I)$ as a function of radius. The solid line marks the mean value between $5''$ and $20''$, which is $A_R/E(R-I) = 3.60$.

In Figure 8, $E(R-I)/A_R$ is plotted against A_R and compared with three model dust distributions. Points at low optical depth are not shown because of their large uncertainties. The solid line is the prediction for the Fitzpatrick reddening law for the spectral energy distribution of a reddened elliptical galaxy obscured exclusively by foreground dust with the characteristics of the diffuse interstellar medium of the Milky Way. In this case, $E(R-I)/A_R$ is 0.25 to 0.26, close to the mean of 0.28, which is observed. The dotted and dashed lines show possible extremes if the dust is embedded in Maffei 1. These have been computed assuming that the dust is confined to a layer of finite thickness centered on the midplane of the galaxy and that stars and dust within the layer are uniformly mixed (see Tully & Fouqué 1985). The dashed curve shows the expected relation if the dust layer is infinitesimally thin compared with the distribution of stars, and the dotted curve shows the relation if the stars are entirely enshrouded. Adopted extinction coefficients are those appropriate for an elliptical galaxy at rest obscured by half the optical depth of the layer (the average optical depth of the stars). The data at high optical depth suggest that a significant fraction of the dust superposed upon Maffei 1 is in the foreground. To explain the observations with dust embedded in Maffei 1 would require a cloud that almost completely enshrouds stars along the line of sight, which is highly unlikely given the small size of the dust lane relative to the galaxy. Although it is possible to

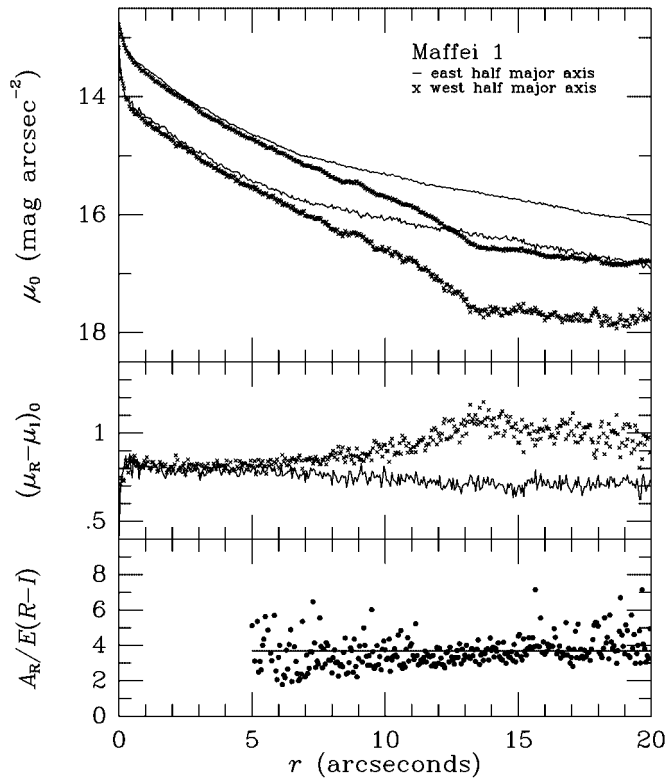

FIG. 7.—*Top*: PC1 surface brightness (*I*, *upper curve*; *R*, *lower curve*) and color profiles of Maffei 1 along the major axis. The two halves of the major axis are displayed differently and are folded around $r = 0''$. *Bottom*: Ratio of total-to-selective extinction, assuming that the east half of the major axis is the unextinguished half (relative to the assumed Galactic extinction.)

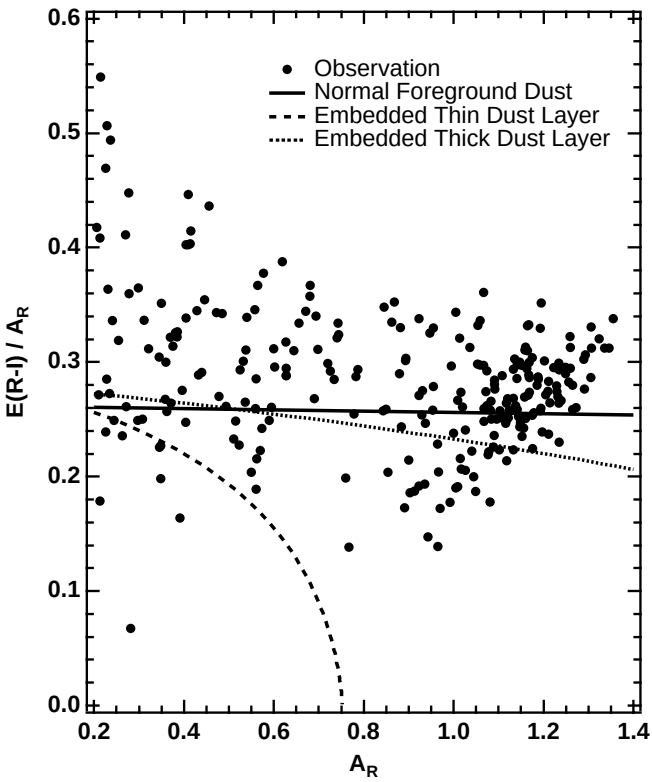

FIG. 8.—Ratio of selective-to-total extinction vs. total extinction for dust features superposed upon Maffei 1, based on the profiles in Fig. 7. The observations (*points*) are compared with the predictions for three different dust distributions (on top of the known foreground dust), assuming that the dust obeys a reddening law typical of that for the diffuse interstellar medium of the Milky Way. Points at $A_R < 0.2$ are particularly uncertain and are not displayed. The solid curve is the relation expected if the features are due to extra dust located entirely in the foreground. The dashed curve arises if the features are due to dust confined to a thin layer inside Maffei 1. The dotted curve is expected if the features are due to dust uniformly mixed with the stars in Maffei 1.

envision a dust layer associated with Maffei 1 that is predominantly in the foreground of the stars, it is more likely that the dust responsible for the excess obscuration seen in the core of the galaxy is actually located in the Milky Way.

Guhathakurta et al. (1999) used *HST* snapshot *V* and *I* images to analyze the extinction toward Maffei 1 in a manner similar to ours but concluded that the ratio of total-to-selective extinction, $A_V/E(V-I)$, is much higher than for a typical Galactic line of sight. They obtained an impossibly high value of this ratio toward Maffei 1 by using the reddening law of Cardelli, Clayton, & Mathis (1989, hereafter CCM). However, Fitzpatrick (1999) showed that the CCM law is inaccurate in *R* and *I*. Our analysis, which accounts properly for effective wavelength shifts, shows that the mean value of $A_R/E(R-I)$ observed in Figures 7 and 8 is very close to that expected for the diffuse component of the interstellar medium of the Milky Way (see McCall 2002). This proves that the line of sight toward Maffei 1 is not unusual, that the reddening law employed by Fingerhut et al. (2003) to derive the extinction is valid, and that the distance and luminosity of Maffei 1 that follow and are adopted in this paper are credible.

4.3. *Core Type of Maffei 1*

We restrict our high-resolution profile analysis to the PC1 field where contamination by foreground stars is minimal and where the signal-to-noise ratio is highest. The task ELLIPSE in the IRAF-based package STSDAS was used to fit ellipses to the F675W and F814W surface brightnesses as a function of radius out to 11.″2. ELLIPSE uses Fourier techniques to measure the intensity, ellipticity, position angle, central coordinates, and $m = 4$ deviations of the light distribution at different radii (Jedrzejewski 1987). The few obvious foreground stars in the PC1 field were masked from the fits with INDEF values. Analysis of the PSF on the images showed that the FWHM is slightly larger on the F814W image than on the F675W image. To match the PSFs on the two images, we used the IRAF task GAUSS, smoothing the F675W image with a Gaussian having $\sigma = 0.65$ dither pixels (0.″015). The sky values derived in § 4.1 were used to eliminate the background. Figure 9 shows the transformed ellipse-fit profiles for an assumed distance of 3.0 Mpc (see also Table 1).

Figure 9 also shows the other fitted ellipse parameters, including the major-axis position angle ϕ, the ellipticity ϵ, the relative amplitude of the $m = 4$ deviation b_4, and the dust-free color index $(R-I)_0$ (i.e., $R-I$ corrected for uniform obscuration with optical depth 1.69 at 1.0 μm), all as a function of radius out to 11.″2 (160 pc). Beyond 0.″1, the color is nearly uniform with $\langle R-I_0 \rangle = 0.81$. According to Buta & Williams (1995), the mean integrated effective $R-I$ color index of an elliptical galaxy is 0.63 ± 0.04, so either the central color is redder than the effective color (which is possible since the effective radius is about 210″; BM99), Maffei 1 is simply redder than is typical of the objects in the

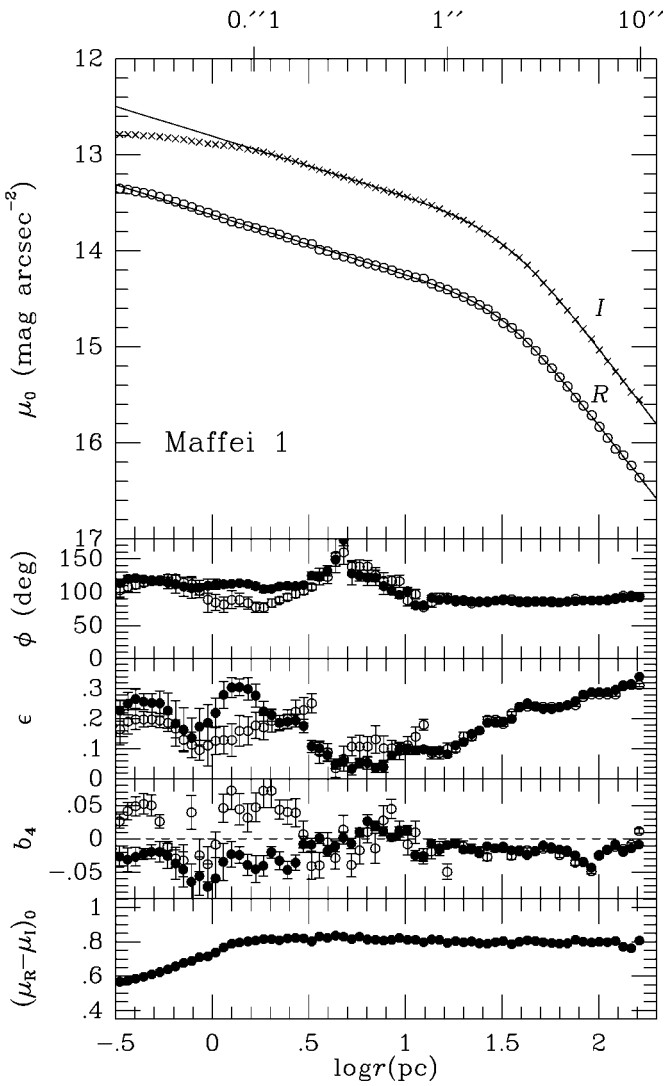

FIG. 9.—Results of fits of free ellipses to the PC1 surface brightness distributions in Maffei 1. *Top to bottom*: Surface brightness μ_0, the fitted major-axis position angle ϕ, the fitted ellipticity ϵ, the relative amplitude b_4 of the $\cos 4\theta$ deviations from a pure ellipse, and the color index $(\mu_R - \mu_I)_0$, each as a function of radius r in parsecs (based on a distance of 3.0 Mpc). Open circles refer to the F675W filter while crosses refer to the F814W filter. *Top*: Nuker law fits to the points having $\log r \geq 0.20$, where r is in parsecs (*solid curves*). The photometry has been corrected for Galactic extinction, assuming an optical depth of 1.69 at 1.0 μm.

sample of Buta & Williams (1995), or both. The mean position angle between 0.″7 and 11″ is 87° ± 4°, and the mean ellipticity over the same radius range is 0.21 ± 0.08, the errors in each case being standard deviations. For comparison, the mean values of these parameters over the whole galaxy are 84° and 0.27, respectively (BM99).

Beyond 0.″6, the parameter b_4 is negative, indicating that Maffei 1 is in the "boxy" elliptical galaxy class (Kormendy & Bender 1996). The Kormendy & Bender classification would be E(b)3. Boxy elliptical galaxies tend to be characterized by little rotation and significant anisotropy in velocity dispersion.

The blueing of the $R-I$ color within 0.″1 appears to be significant. It is associated with the nuclear point source as shown in Figure 4 (*right*). It is not due to PSF differences between the R and I filters because we have corrected for any mismatch. To evaluate how much might be due to Hα contamination, we derived an Hα-free R-band image by iteratively computing a continuum-free Hα image and subtracting it. At most, Hα emission makes the $R-I$ color in the center too blue by 0.15 mag. The mean corrected color of 0.81 outside the blueing zone differs by 0.3 mag from the central color of 0.50. Thus, Hα contamination in the F675W filter accounts for about half of the observed decline.

Figure 10 shows a composite I-band profile of Maffei 1 corrected for Galactic extinction plotted versus $r^{1/4}$. The points having $r^{1/4} \leq 1.8$ (where $r \leq 11''$) are based on the PC1 while those at larger radii are from Table 9 of BM99. The BM99 values were corrected for an extinction of $A_I = 2.65$ mag (Fingerhut et al. 2003). The solid line in Figure 10 is from Table 10 of BM99. The plot shows that surface brightnesses within $r = 16''$ depart from the $r^{1/4}$ law defined by the outer points.

The profiles in Figure 9 can be used to determine the core type of Maffei 1. Lauer et al. (1995) discuss the core paradigm for early-type galaxies. *Power-law galaxies* have profiles that are more or less consistent with a single power law over the central region, whereas *core galaxies* have an inner zone where the outer power law breaks and decreases in slope. To quantify the distinction, Lauer et al. fitted Nuker profiles to the surface brightness distributions of 45 elliptical galaxies and bulges. Nuker profiles are analytical models of the form

$$I(r) = 2^{(\beta-\gamma)/\alpha} I_b \left(\frac{r_b}{r}\right)^{\gamma} \left[1 + \left(\frac{r}{r_b}\right)^{\alpha}\right]^{(\gamma-\beta)/\alpha},$$

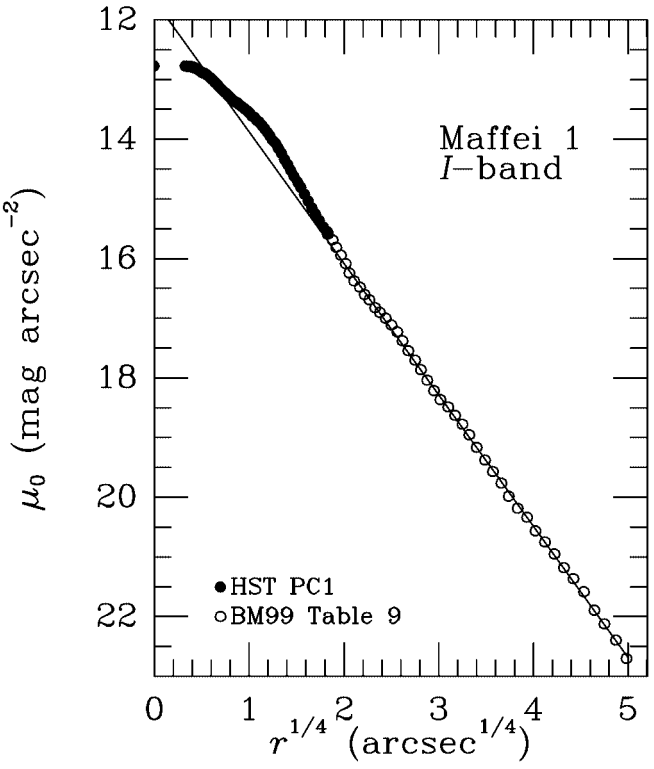

FIG. 10.—Composite extinction-corrected luminosity profile of Maffei 1 in I. Points were derived by fitting free ellipses to the surface brightness distribution. Those for $r^{1/4} \leq 1.8$ are based on the PC1 results, while the remainder are from BM99.

TABLE 1
SURFACE PHOTOMETRY OF MAFFEI 1[a]

r (arcsec)	μ_I^0 (mag arcsec^{-2})	$(\mu_R-\mu_I)_0$ (mag arcsec^{-2})	r (arcsec)	μ_I^0 (mag arcsec^{-2})	$(\mu_R-\mu_I)_0$ (mag arcsec^{-2})
0.000	12.77	0.50	0.362	13.26	0.82
0.012	12.77	0.52	0.399	13.28	0.83
0.013	12.77	0.52	0.439	13.32	0.81
0.014	12.78	0.54	0.482	13.34	0.81
0.016	12.78	0.54	0.531	13.37	0.81
0.017	12.78	0.55	0.584	13.39	0.81
0.019	12.78	0.56	0.642	13.41	0.82
0.021	12.78	0.56	0.706	13.44	0.81
0.023	12.79	0.57	0.777	13.47	0.81
0.025	12.79	0.57	0.855	13.49	0.80
0.028	12.79	0.59	0.940	13.53	0.81
0.030	12.80	0.60	1.034	13.56	0.81
0.033	12.81	0.61	1.137	13.61	0.79
0.037	12.81	0.62	1.251	13.64	0.80
0.040	12.82	0.64	1.376	13.68	0.80
0.045	12.83	0.66	1.514	13.72	0.80
0.049	12.84	0.68	1.665	13.77	0.79
0.054	12.86	0.69	1.832	13.82	0.79
0.059	12.87	0.71	2.015	13.88	0.80
0.065	12.88	0.72	2.217	13.95	0.80
0.072	12.89	0.74	2.438	14.02	0.79
0.079	12.90	0.77	2.682	14.07	0.80
0.087	12.91	0.79	2.950	14.15	0.81
0.095	12.92	0.79	3.245	14.24	0.80
0.105	12.94	0.80	3.570	14.34	0.80
0.115	12.95	0.81	3.927	14.43	0.79
0.127	12.97	0.82	4.320	14.53	0.79
0.140	12.99	0.81	4.752	14.62	0.79
0.154	13.02	0.81	5.227	14.72	0.81
0.169	13.04	0.82	5.749	14.81	0.80
0.186	13.07	0.82	6.324	14.92	0.80
0.205	13.10	0.82	6.957	15.03	0.80
0.225	13.13	0.80	7.653	15.15	0.80
0.248	13.16	0.83	8.418	15.26	0.80
0.272	13.18	0.82	9.260	15.36	0.77
0.300	13.21	0.84	10.186	15.47	0.76
0.329	13.23	0.83	11.204	15.55	0.81

[a] Photometric parameters are corrected for Galactic extinction amounting to an optical depth of 1.69 at 1 μm (Fingerhut et al. 2003). The corresponding extinctions adopted for A_{F675W} and A_{F814W} were 3.51 and 2.63 mag, respectively. Being based on the drizzled images, the pixel size is 0.″02275. A step factor of 1.1 was used with IRAF routine ELLIPSE.

where r is the radius, r_b is a break radius, I_b is the intensity at this radius, and α, β, and γ describe the shape of the profile. We fitted this law to the extinction-corrected profiles in Figure 9 by using nonlinear least squares. Only points with $r \geq 0.''11$ were used for the fits, because the Nuker law cannot fit the whole I-band profile. Table 2 summarizes the parameters of the Nuker law so derived. According to Lauer et al. (1995), an early-type galaxy is considered to be a power-law type if $\gamma > 0.5$, whereas it is considered to be a core type if $\gamma < 0.3$. Table 2 shows that Maffei 1 has $\gamma = 0.25$ in both *HST* filters, meaning it is a core-type elliptical galaxy. This is typical mainly of luminous elliptical galaxies (Faber et al. 1997). The break radius of 34 pc is comparable to values for elliptical galaxies such as NGC 1400 and NGC 3608 (Faber et al. 1997), which have absolute magnitudes $M_V^0 \approx -21$. However, the values of α, β,

TABLE 2
NUKER LAW FITS TO THE SURFACE BRIGHTNESSES IN MAFFEI 1[a]

Filter	α	β	γ	I_b ($L_\odot$ pc^{-2})	r_b (pc)
F675W	3.26 ± 0.19	1.026 ± 0.013	0.249 ± 0.003	33317 ± 424	32.8 ± 0.6
F814W	2.81 ± 0.16	1.063 ± 0.015	0.249 ± 0.004	49050 ± 747	33.9 ± 0.7

[a] Restricted to radius range $0.''11 \leq r \leq 11.''2$, which corresponds to 1.6 pc $\leq r \leq$ 160 pc, for a distance of 3.0 Mpc.

and γ for Maffei 1 are more comparable to those for M87 than for NGC 1400 and NGC 3608.

The solid curves in Figure 9 show that the Nuker law fits the central luminosity distribution in Maffei 1 extremely well over the range 1.6 to 160 pc. The same fit also represents the innermost parts of the *R*-band profile well. However, inside 1.6 pc the *I*-band profile deviates substantially below the extrapolated Nuker fit. This is the region where the $R-I$ color also decreases, and spans only $\approx$4 dither pixels radius.

5. GLOBULAR CLUSTER CANDIDATES IN MAFFEI 1

Inspection of the four CCD fields in our Maffei 1 images reveals a small number of slightly diffuse round objects that are candidates for globular clusters. These were identified by their slightly or obviously extended images compared with foreground stars. The most obvious candidates were identified through simple visual inspection, while additional candidates were found by fitting the (well sampled) stellar point-spread function to all starlike sources. All extended objects showed a characteristic ring-shaped pattern in the residuals. We identified 20 candidate clusters, 19 of which are labeled in Figure 11. Perhaps in part because of the extremely bright background, only one candidate was identified in the PC1 field. This candidate (object 20) is indicated in Figure 12.

As a check that these objects are slightly diffuse, we also computed concentration parameters $\Delta I(0.5\text{–}3)$, the difference in *I*-band magnitude between a circular aperture of radius 0.5 pixel and one of radius 3 pixel (see Miller et al. 1997), for 132 nonsaturated stellar sources on the drizzled WF frames, and a similar parameter, $\Delta I(1\text{–}6)$, for 24 sources in the PC1 frame. The average values found for these parameters are $\langle \Delta I(0.5\text{–}3) \rangle = 2.59 \pm 0.03$ mag (stand. dev. = 0.36 mag) and $\langle \Delta I(1\text{–}6) \rangle = 2.22 \pm 0.05$ mag (stand. dev. = 0.23 mag). The mean value of ΔI for the 20 globular cluster candidates is 2.99 ± 0.04 mag (stand.

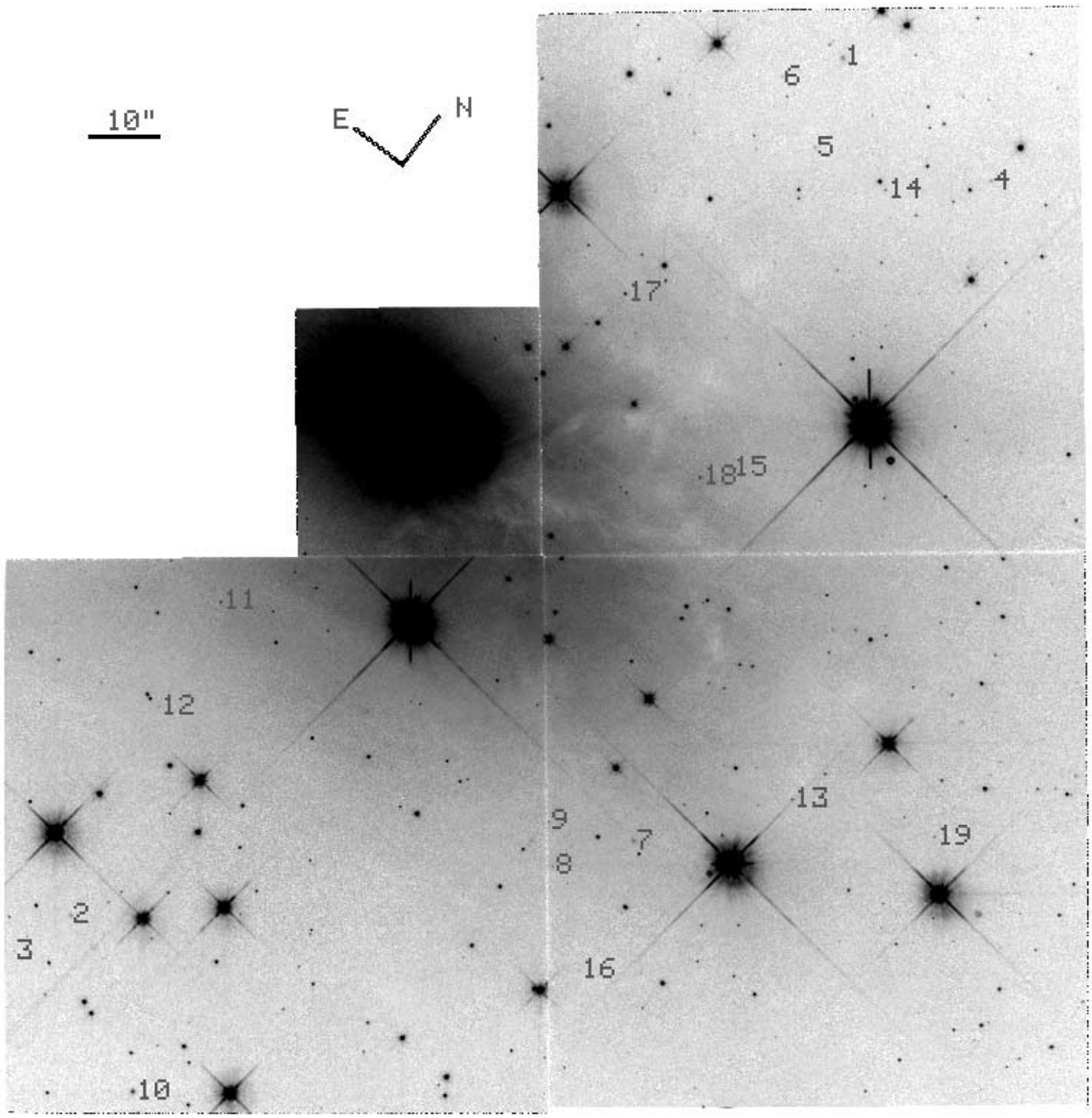

FIG. 11.—Mosaic image of the full WFPC2 field of Maffei 1. The numbered objects are candidate globular clusters. Photometry for these objects is presented in Table 3.

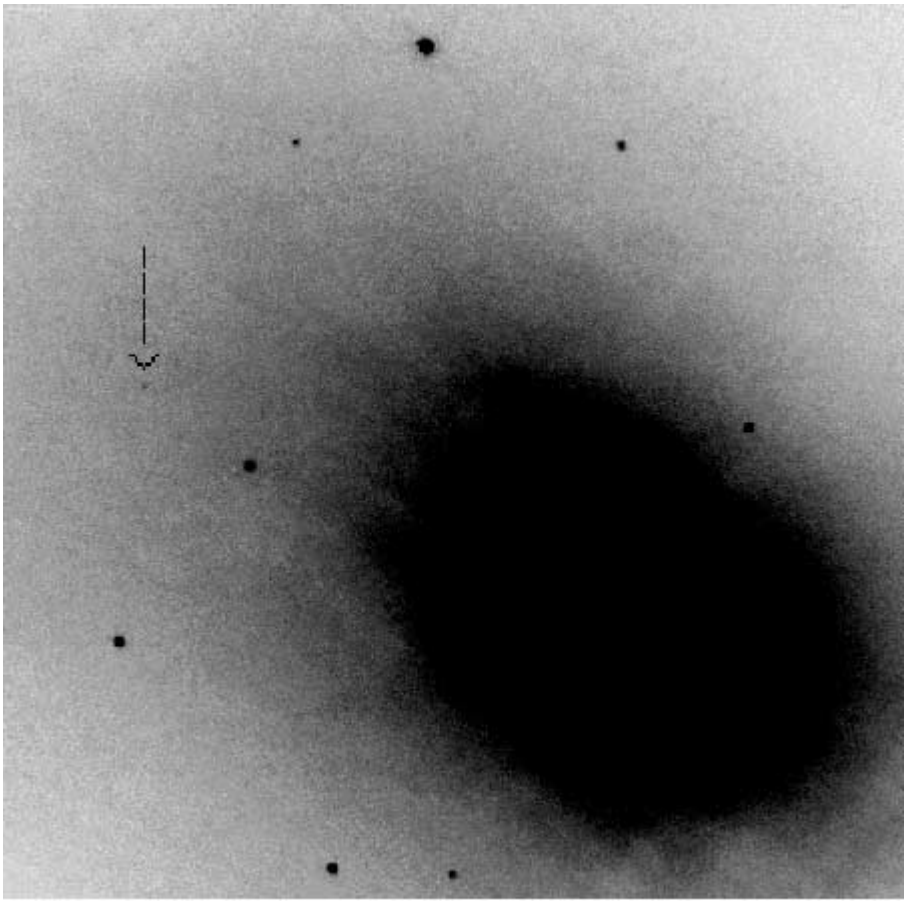

FIG. 12.—Single globular cluster candidate (*arrow*) in the PC1 field. The arrow is 3.″23 in length. The orientation of the image is the same as in Fig. 11.

dev. = 0.19 mag). The concentration values are listed in Table 3 for each candidate.

Total magnitudes and colors were derived using the IRAF routine PHOT. Because the cluster candidates were found mainly in the WF frames, we made corrections for charge transfer efficiency following the procedure outlined in Whitmore et al. (1999) for a 2 pixel radius aperture (equivalent to 4 pixels on the drizzled images). Total magnitudes were derived by determining aperture corrections to 5–10 WF pixel radius. It was not possible to use a single mean growth curve for these corrections because the clusters have widely differing sizes. For example, objects 1 and 10 have diameters between 1″ and 2″ in I, despite 2.65 mag extinction. Thus, aperture corrections ranged from 0.36 to 1.60 mag.

Table 3 lists the derived magnitudes and colors, corrected for uniform foreground extinction. The brightest object in the field is No. 10 (Fig. 13), whose corrected color is $(R-I)_0 = 0.58$. Assuming its intrinsic $V-I$ color is equal to the mean value of 1.1 found for other extragalactic globular cluster systems (Illingworth 1996), we estimate an absolute magnitude of $M_V^0 = -8.5$, comparable to M3 (Madore 1980).

The most diffuse object we have identified is labeled No. 1 and is located 77.″7 nearly due north of the nucleus in position angle 348.°2. The object (Fig. 14) shows a resolved core with an obvious diffuse envelope 1.″0 in radius. Within this radius, the object has a corrected magnitude $I_0 = 18.31$ and a corrected color $(R-I)_0 = 0.90$, redder than the integrated light of Maffei 1 itself. If it is a metal-rich globular cluster, its unusual color could be a consequence of its location in a dusty area in the WFPC2 field.

Figure 15 shows the ($R-I$, I) color-magnitude diagram for the 20 candidates, as well as for Galactic globular clusters (Harris 1996). Besides having a wider color spread, most of the candidates appear to be redder than the majority of clusters in the Milky Way. The weighted mean $R-I$ color is 0.62 ± 0.05 while the mean Galactic $R-I$ color is 0.48 ± 0.06. If the globular clusters in Maffei 1 are not excessively obscured, then the difference could signify that the Maffei 1 globular clusters are more metal-rich on average than the Galactic ones, at least in the inner zone covered by the small WFPC2 field. That this may partly explain the difference is evidenced by the mean $R-I$ color of the 20 Galactic globular galaxies having $[\mathrm{Fe/H}] \geq -1$, which is 0.55 ± 0.06. On the other hand, the spread in the colors of the candidate clusters also suggests that the extinction is variable across the field. Variable extinction could also explain the redward bias in the mean color relative to the Milky Way globular clusters. The second-brightest object, No. 17, is nearly as bright as object No. 10 but has an $R-I$ color 0.24 mag redder than object 10. Object 17 appears near the edge of a faint but distinct dust lane. Note that if reddening lines are followed back to the main concentration of globular clusters in the Milky Way, all the redder candidates remain within the absolute magnitude range of the Galactic clusters.

TABLE 3
PHOTOMETRY OF CANDIDATE GLOBULAR CLUSTERS IN MAFFEI 1

Object (1)	α, δ (J2000.0) (2)	I_0 (3)	$(R-I)_0$ (4)	M_I^0 (5)	ΔI (6)
1	2 36 33.30, 59 40 33.56	18.31 ± 0.06	0.90 ± 0.08	−9.1	3.18
2	2 36 35.26, 59 37 55.56	19.32 ± 0.04	0.08 ± 0.09	−8.1	3.17
3	2 36 35.70, 59 37 46.89	20.70 ± 0.06	0.72 ± 0.19	−6.7	2.65
4	2 36 29.80, 59 40 32.22	19.60 ± 0.04	0.47 ± 0.11	−7.8	3.21
5	2 36 32.74, 59 40 21.41	19.74 ± 0.04	0.41 ± 0.10	−7.7	2.82
6	2 36 33.99, 59 40 26.46	20.40 ± 0.05	0.55 ± 0.14	−7.0	2.91
7	2 36 27.86, 59 38 50.07	19.01 ± 0.03	0.82 ± 0.07	−8.4	3.23
8	2 36 28.76, 59 38 40.55	19.55 ± 0.07	0.48 ± 0.12	−7.8	3.16
9	2 36 29.30, 59 38 45.19	20.15 ± 0.12	0.90 ± 0.19	−7.2	2.89
10	2 36 32.45, 59 37 41.23	17.77 ± 0.02	0.58 ± 0.04	−9.6	3.04
11	2 36 36.48, 59 38 42.38	19.13 ± 0.03	0.41 ± 0.06	−8.3	2.87
12	2 36 36.24, 59 38 25.69	20.57 ± 0.09	0.62 ± 0.16	−6.8	2.85
13	2 36 25.99, 59 39 07.70	19.23 ± 0.03	0.61 ± 0.07	−8.2	2.80
14	2 36 31.25, 59 40 22.54	19.49 ± 0.04	0.50 ± 0.08	−7.9	3.11
15	2 36 30.49, 59 39 39.17	20.13 ± 0.09	1.36 ± 0.19	−7.3	3.09
16	2 36 27.26, 59 38 31.36	20.95 ± 0.13	0.10 ± 0.24	−6.4	3.33
17	2 36 33.92, 59 39 49.66	18.14 ± 0.03	0.83 ± 0.05	−9.3	2.94
18	2 36 30.83, 59 39 35.58	18.76 ± 0.02	0.63 ± 0.05	−8.6	2.92
19	2 36 23.50, 59 39 15.23	19.92 ± 0.06	0.74 ± 0.10	−7.5	2.67
20	2 36 37.35, 59 39 15.07	20.01 ± 0.07	0.75 ± 0.15	−7.4	3.01

NOTES.—Units of right ascension are hours, minutes, and seconds, and units of declination are degrees, arcminutes, and arcseconds. Col. (3): I-band total magnitude; col. (4): $R-I$ color index; col. (5): absolute I-band total magnitude, for a distance of 3.0 Mpc; col. (6): concentration parameter $\Delta I(0.5–3)$ for objects 1–19 and $\Delta I(1–6)$ for object 20 (see text). A subscript or superscript of zero on the photometric parameters means that these are corrected for Galactic extinction. The extinction values used were $A_{F675W} = 3.52$ mag and $A_{F814W} = 2.64$ mag, assuming most of the clusters are metal-poor.

To determine whether the sizes and concentrations of the Maffei 1 objects are consistent with those for known globular clusters, we have fitted analytical King models to the integrated luminosity profiles of the three brightest candidates. The PSF was accommodated by convolving each model with a Gaussian having standard deviation $\sigma = 1.2$ dither pixels (0.″06). The results are summarized in Table 4. In each case, we are able to find a Galactic

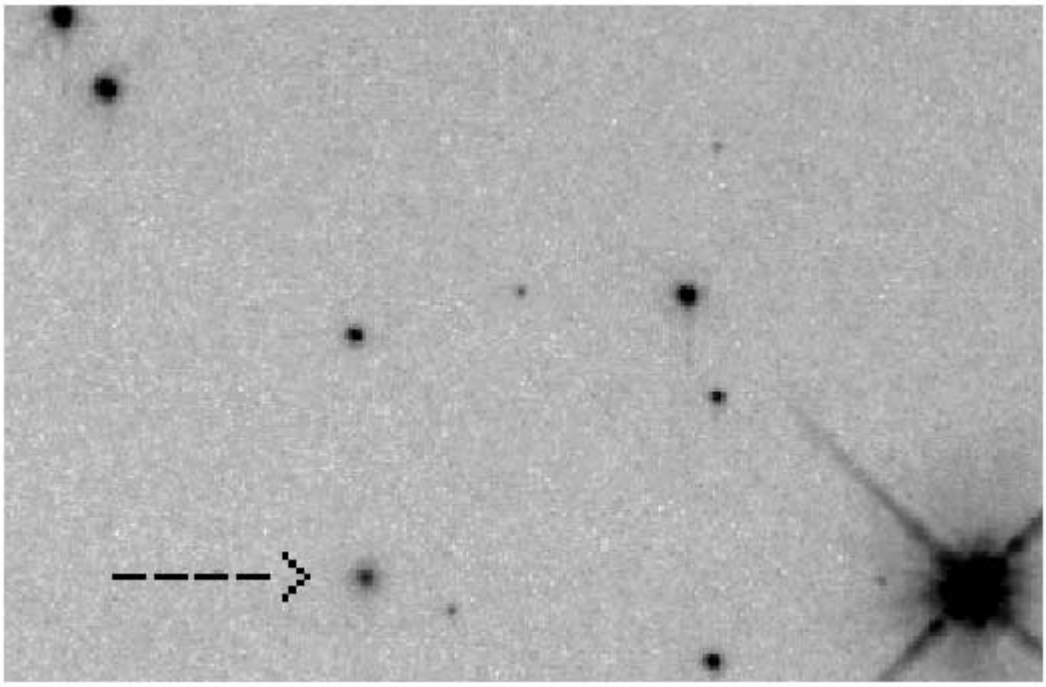

FIG. 13.—Small part of WFPC2 field (filter F814W), showing the brightest candidate globular cluster in I, No. 10 (*arrow*). The field lies approximately 100″ south and slightly west of the center of Maffei 1 in frame WF2 (see Fig. 11). The arrow is 4.″25 in length. North is approximately to the upper right, and east is approximately to the upper left, as in Fig. 11.

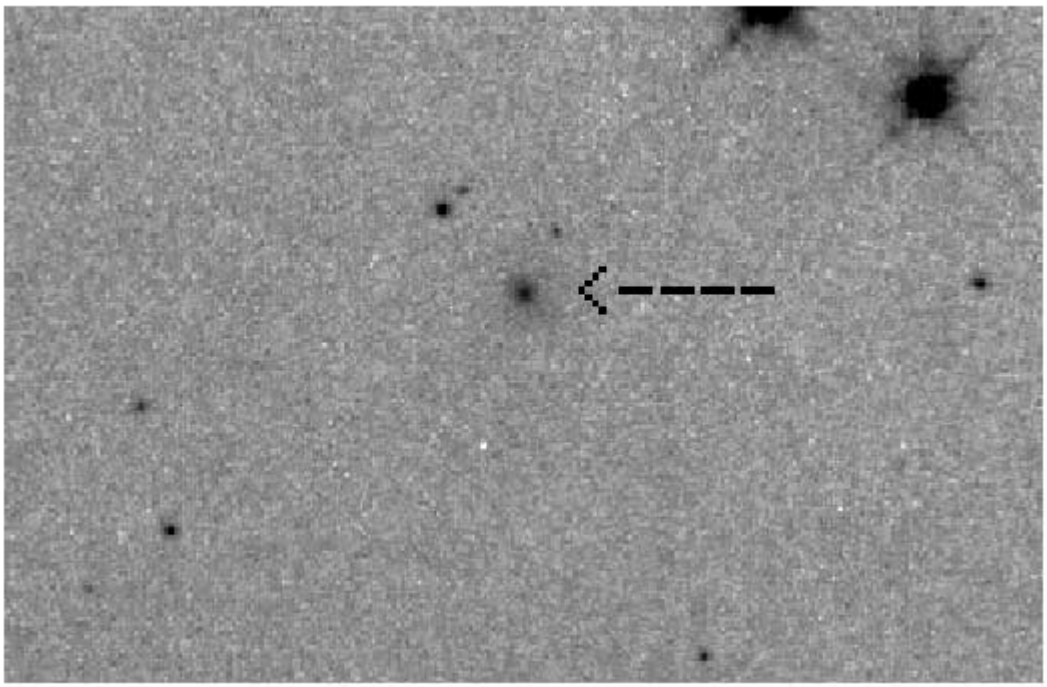

FIG. 14.—Small part of WFPC2 field (filter F814W) showing the most diffuse candidate globular cluster, No. 1 (*arrow*). The field lies approximately 78″ north and slightly west of the center of Maffei 1 in frame WF4 (see Fig. 11). The arrow is 4.″25 in length. North is approximately to the upper right, and east is approximately to the upper left, as in Fig. 11.

globular whose structural parameters are similar to those of the candidate.

6. CONCLUSIONS

We have shown that Maffei 1 is a core-type elliptical galaxy having a break radius of 34 pc. Its nuclear parameters are typical of a luminous elliptical galaxy with absolute magnitude $M_V^0 \approx -21$. Departures from a Nuker law profile within $r = 1.6$ pc signify either a change in stellar population or the influence of a nonstellar continuum source, even after allowing for some contamination by Hα.

The WFPC2 field of Maffei 1 shows considerable variable extinction. By assuming that the east side of Maffei 1 approximates the shape of the extinction-free profile, we have deduced that the large dust patch 15″ west of Maffei 1 is Galactic in origin.

Hα emission from Maffei 1 appears to come almost entirely from a source in the nucleus only 1.2 pc across. The emission is confined to a region where the $R-I$ color index is bluer than the extranuclear value, even after allowing for Hα contamination of the $R-I$ color. This source contains only about 29 $M_\odot$ of ionized gas.

We have identified 20 slightly or obviously diffuse sources. We suspect that most of these sources are globular clusters associated with Maffei 1. If correct, the brightest cluster would have an absolute magnitude $M_V^0 = -8.5$ for a distance of 3.0 Mpc, comparable to M3.

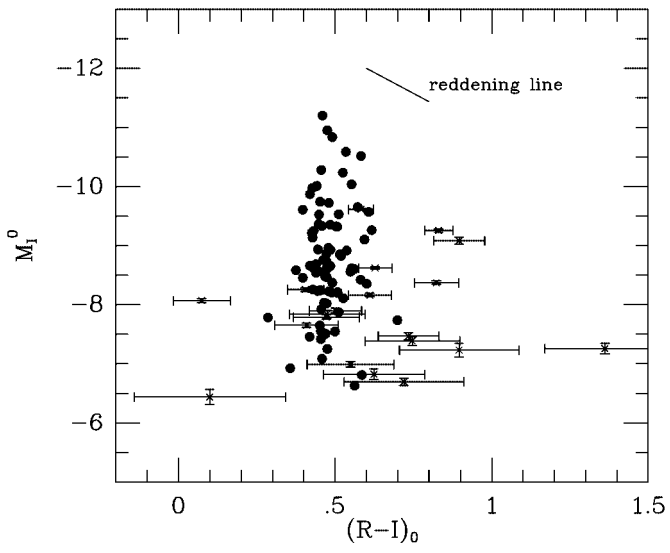

FIG. 15.—Color-magnitude diagram for 20 diffuse objects in the WFPC2 field of Maffei 1. Shown for comparison is the color-magnitude diagram for Galactic globular clusters from Harris (1996).

TABLE 4

CORE RADII AND CONCENTRATION PARAMETERS FOR THREE CANDIDATES COMPARED WITH GALACTIC GLOBULAR CLUSTERS[a]

Object	r_c (pc)	$c = \log(r_t/r_c)$	M_I^0
Maffei 1 No. 1	2.4	1.50	−9.1
NGC 7006	2.9	1.42	−8.6
Maffei 1 No. 10	1.1	1.80	−9.6
M2	1.1	1.80	−9.9
Maffei 1 No. 17	1.0	1.05	−9.3
NGC 6553	0.9	1.17	−9.3

[a] Parameters for NGC 6553, NGC 7006, and M2 are from Harris 1996.

The existence of the central Hα source and the small size of the nucleus allows the possibility of future studies of the dynamics of Maffei 1 that probe much deeper into the core than has been possible for any other giant elliptical galaxy. In spite of the high extinction, such studies should be feasible.

We thank Karl Gebhardt for helpful discussions. R. B. acknowledges the support of NASA STScI grant GO 8101 to the University of Alabama. M. L. M. acknowledges the support of the Natural Sciences and Engineering and Research Council of Canada.

REFERENCES

Buta, R., & McCall, M. L. 1983, MNRAS, 205, 131
———. 1999, ApJS, 124, 33 (BM99)
Buta, R., & Williams, K. L. 1995, AJ, 109, 543
Cardelli, J., Clayton, G., & Mathis, J. 1989, ApJ, 345, 245 (CCM)
de Vaucouleurs, G. 1975, in Galaxies and the Universe: Stars and Stellar Systems, Vol. 9, ed. A. Sandage, M. Sandage, & J. Kristian (Chicago: Univ. Chicago Press), 557
Faber, S. M., et al. 1997, AJ, 114, 1771
Fingerhut, R., McCall, M. L., De Robertis, M., Kingsburgh, R. L., Komljenovic, M., Lee, H., & Buta, R. J. 2003, ApJ, 587, in press
Fitzpatrick, E. L. 1999, PASP, 111, 63
Ford, H. C., & Jenner, D. C. 1971, ApJ, 165, L1
Goudfrooij, P. 1995, PASP, 107, 502.
Guhathakurta, P., et al. 1999, BAAS, 195(805)
Harris, W. E. 1996, AJ, 112, 1487
Holtzman, J. A., Burrows, C. J., Casertano, S., Hester, J. J., Trauger, J. T., Watson, A. M., & Worthey, G. 1995, PASP, 107, 1065
Illingworth, G. D. 1996, in Science with the *Hubble Space Telescope* II, ed. P. Benvenuti, F. Macchetto, & E. J. Schreier (Baltimore: STScI), 79
Jedrzejewski, R. 1987, MNRAS, 226, 747
Kormendy, J., & Bender, R. 1996, ApJ, 464, L119
Krismer, M., Tully, R. B., & Gioia, I. 1995, AJ, 110, 1584
Lauer, T., et al. 1995, AJ, 110, 2622
Luppino, G. A., & Tonry, J. L. 1993, ApJ, 410, 81
Madore, B. 1980, in Globular Clusters, ed. D. Hanes & B. Madore (Cambridge: Cambridge Univ. Press), 21
Maffei, P. 1968, PASP, 80, 618
McCall, M. L. 2002, ApJ, submitted
Miller, B. W., Whitmore, B. C., Schweizer, F., & Fall, S. M. 1997, AJ, 114, 2381
Phillips, M. M., Jenkins, C. R., Dopita, M. A., Sadler, E. M., & Binette, L. 1986, AJ, 91, 1062
Spinrad, H., et al. 1971, ApJ, 163, L25
Tully, R. B., & Fouqué, P. 1985, ApJS, 58, 67
Whitmore, B., Heyer, I., & Casertano, S. 1999, PASP, 111, 1559